Remote Sensing Contribution to the Detection of Karst Features and their structural Environment in the Area of the Bekaa Valley in Central-Lebanon

Barbara Theilen-Willige[*]

Retired from Technische Universität Berlin (TU), Berlin, Germany. Email: Barbara.Theilen-Willige@t-online.de[*]

ABSTRACT

More than two-thirds of the area of Lebanon is covered by lime-and dolostones prone to karst processes, and, thus, developed surface karst features, such as poljes, dolines, uvalas, caves, and blind valleys. This study aims to map the surface karst features, especially sinkholes, and to identify their orientation and dimensions, as well as the tectonic pattern influencing their development based on remote sensing data and references. As karst affected areas are at a higher risk of environmental pollution of the aquifers in the densely populated area due to the karst specific surface and subsurface drainage conditions, the knowledge of the structural pattern and fault systems influencing surface infiltration and groundwater flow is important. This study is focused on the evaluation of optical satellite data (Landsat, Sentinel 2) as well as of radar images (Sentinel 1, ALOS PALSAR) and on Digital Elevation Model (DEM) data (SRTM, ASTER, ALOS PALSAR) and DEM derived morphometric maps aiming to detect traces of karst features, fault zones and their related structures, combined with other geoscientific data of Central-Lebanon. DEM derived maps support the detection of areas with higher surface water input due to their specific local morphometric disposition. The evaluations of the different data sets clearly show that sinkholes and springs in Central-Lebanon are concentrated along a nearly semi-circular belt along western part of the left-lateral Yammouneh shear fault zone. The main factors influencing the occurrence and distribution of surface karst features could be derived by the combined analysis of remote sensing data and reference information.

Keywords: Karst features; Tectonic pattern; Brittle surfaces; Remote sensing; Earthquakes; Morphometric maps; Hydrogeology; Bekaa Valley; GIS; Central-Lebanon.

1. Introduction

More than two-thirds of the area of Lebanon are prone to karstification processes including surface karst features such as poljes, uvalas, dolines, blind valleys, natural bridges, as well as smaller features like karren [1]. Subsurface karst features comprise many types of solutional shafts and galleries, caves, subsurface lakes and rivers and most types of speleothems. The Jurassic, Cretaceous and Eocene limestones /dolomites form the core of the Lebanon ranges [2]. Sinkholes play a major role in recharging amounts of groundwater, mainly from the melting snow covering the Lower Jurassic and Upper Cretaceous (Cenomanian) rocks several months a year. The groundwater recharge process in the area benefits as well from rainfall events [1]. Sinkholes and closed depressions are used as detention basins and ponds since decades and, thus, are important for the water supply and water management.

The development of karst phenomena, the intensity and depth of karstification are influenced by various geodynamic movement such as uplift/subsidence or folding, by the structural pattern and by volcanic activities [3]. The pattern of zones of secondary porosity such as faults and fracture zones are controlling factors of the groundwater flow and, thus, of the karst development in the investigation area.

1.1. Study Objectives

This study aims to contribute to the mapping of the surface karst features, especially sinkholes, and to identify their orientation, concentrations and dimensions, as well as the tectonic pattern and further factors influencing their

development, based on remote sensing and GIS derived data and references. A systematic GIS approach aims to gather those factors, to study their complex interactions, and to create a GIS data base.

Of course, the evaluation capabilities of satellite data are limited, and additional research is required to clarify the character and properties of the mapped karst features. This is a requirement for land use planning as the collapse of dolines or caves might be a risk for settlements and the infrastructure. Therefore, one goal of this study is to provide hints and point out directions where future field research or other surveys could be focused.

2. Materials and Methods

This study is dealing with the evaluation of optical satellite data as well as of radar images and of Digital Elevation Model (DEM) data and DEM derived morphometric maps, aiming to detect surface traces of karst features, fault zones and their related structures, combined with other geoscientific data of Central-Lebanon. The evaluations of different satellite data and available geodetic and geophysical data were carried out as summarized in Figure 1.
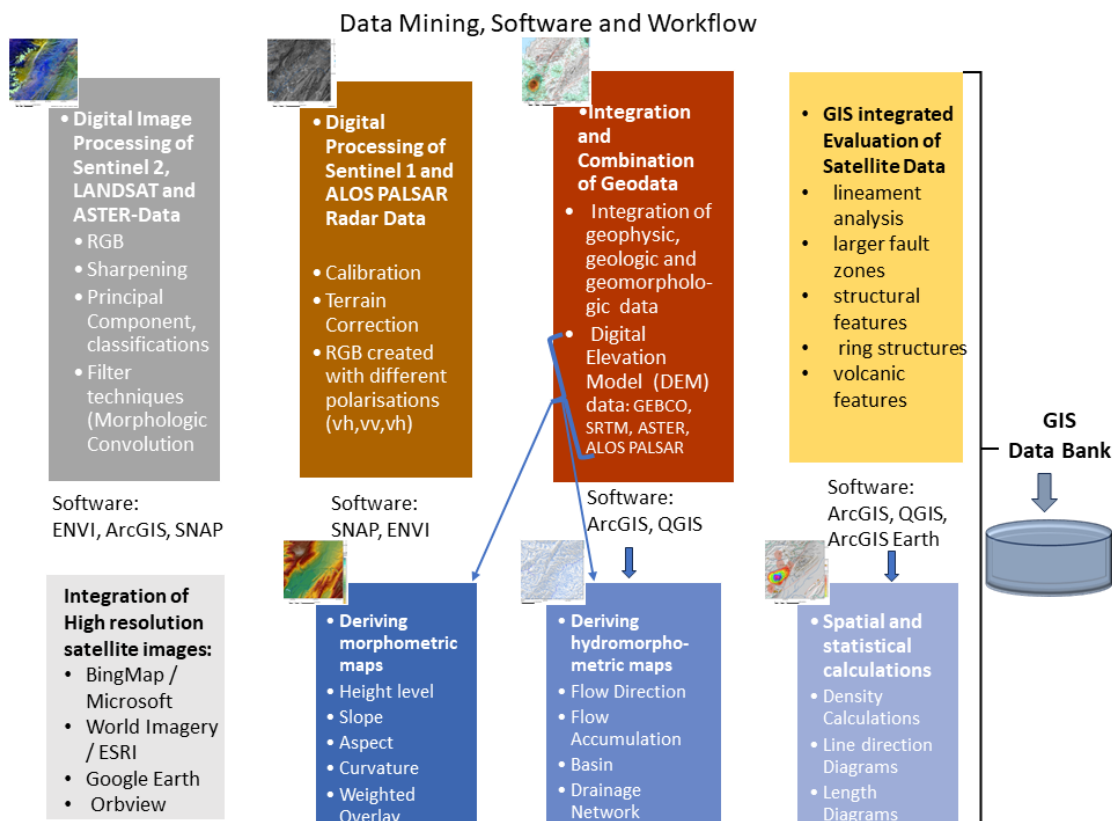
Figure 1. Materials, software, and workflow.

Various factors and parameters derived from thematic layers gained from satellite data and references such as lithology, structural lineaments, terrain analysis and earthquakes were combined in a GIS data base to achieve additional knowledge or to contribute to a better understanding of the known facts.

2.1. Optical Satellite Data

Digital image processing of Landsat TM and 8/9 (the Operational Land Imager (OLI), Sentinel 2 and ASTER data was carried out by merging different Red Green Blue (RGB) band combinations. Special attention was focused on

the creation of RGB images including Landsat 8/9 thermal bands 7 and 10 and ASTER thermal bands (10-14). Filter tools were used for the structural analysis of Landsat and Sentinel 2 data. Sentinel 2 data were included into the data sets. As digital image processing software served the Sentinel Application Platform (SNAP)/ESA and ENVI/L3Harris Geospatial Solutions as well as the processing tools integrated into the geoinformation systems ArcGIS/ESRI and QGIS. The specific digital image processing methods of the different satellite data and image enhancements methods are focused on gaining additional knowledge about the structural pattern such as the filter techniques. The data were provided by the USGS Earth Explorer [4], the ESA Copernicus Browser [5], and the NASA Earth Data [6].

The high-resolution satellite images such as OrbView-3 images, Bing Map from Microsoft and Google Earth images as well the World Imagery data from ArcGIS Earth from ESRI were used as base for detailed mapping.

2.2. Radar Data

Sentinel 1 Synthetic Aperture Radar (SAR, C-Band radar wavelength), ALOS PALSAR (L-Band, 23.5 cm wavelength) radar data were digitally processed and evaluated. The Advanced Land Observing Satellite (ALOS), Phased Array type L-band Synthetic Aperture Radar (PALSAR) from the Japan Aerospace Exploration Agency (JAXA) [7] provided data with 12.5 m spatial resolution. The Sentinel 1 and ALOS PALSAR radar missions included dual polarization capabilities. The radar system can transmit a signal in a horizontal (h) or vertical (v) polarization, and then receive in both h and v polarizations. RGB- tools were used to merge radar images with different polarizations and, thus, get "false-colored" radar images improving the evaluation possibilities, for example by Sentinel 1-vh, vv, vh polarization composites. The different radar wavelengths correlated with the L-Band (23.5 cm) and C-Band (5.6 cm) allow varying radar penetration depths into the surface.

The illumination geometry of the radar signals plays an important role for the visibility of the linear and structural features, especially in the Central-Lebanon area with its high mountain ranges oriented in SSW-NNE direction, creating effects as well like radar image distortions like layover and radar foreshortening. Those oriented perpendicular to the radar illumination angle appear enhanced, whereas those parallel to the radar illumination are more suppressed, return large amounts of the transmitted energy to the radar satellite sensors (visible in light gray tones), while smooth surfaces scatter the energy and, thus, have low radar returns such as the Bekaa valley bottom (appearing dark on the radar images). Other factors such as dielectric properties and radar characteristics (frequency, depression angle, polarization) also affect the radar return [8], [9]. The processing of the radar data was carried out using the SNAP software of ESA and the image processing tools integrated in ArcGIS.

The radar data were provided by the ESA Copernicus Browser [5], and NASA Earth Data, Alaska Satellite Facility (ASF) [10], [11]. ALOS PALSAR mosaics (25 m-resolution) were retrieved from the Earth Observation Research Center, PALSAR global mosaic and Forest/Non-forest Map, JAXA [7].

2.3. DEM Data

Digital Elevation Model (DEM) data (SRTM, ASTER and ALOS PALSAR) and the DEM derived morphometric maps were included into these investigations in a GeoInformation System (GIS) embedded environment.

Morphometric maps like height level and slope gradient maps support the detection of deformation structures along major fault zones. The position of slopes oriented towards wind-driven, rain-bearing clouds has an impact on the intensity of karst development. Therefore, aspect maps derived from DEM data were used to provide information about the orientation of slopes.

For the detection of areas with a relatively higher surface water input the Hydrology tools of ESRI were used to calculate the drainage system (stream order) and flow accumulation as well as the drainage basins based on the DEM data. Weighted overlay tools were used to find areas where the susceptibility to higher surface water input (up to flash floods) is higher due to the accumulation of specific morphometric properties such as the lowest local height level, low slope gradients, no curvature of the terrain or high flow accumulation values.

2.4. Structural Analysis

Shapefiles were created in ArcGIS related to karst features, surface properties, faults and to structural features. Based on the different satellite data a visual lineament and structural analysis was carried out. The visibility of linear features depends on the specific properties of the satellite systems such as their spatial and radiometric resolution, but also on the acquisition time. The seasonal and climatic conditions, as for example the phenological situation of the vegetation, soil moisture conditions, sun elevation, illumination angle and direction at the acquisition time of the satellite data play an important role. The detailed inventory of the surface-near fault and fracture pattern helps to detect those areas, where the permeability of the lime- and dolostones is relatively higher, supporting intrusion and infiltration of meteorological surface water after heavy rains. Special attention was directed at distinct expressed linear features (tonal linear anomalies, geomorphologic linear features, drainage segments, etc.). In the scope of this study the following types of linear and curvi-linear features were mapped: lineaments (as a neutral term for linear features without precisely knowing their origin, fault zones, and structural features. The visual lineament analysis was chosen because it allows the differentiation of several types of linear features what is not possible when using automatic lineament extraction in this high mountain environment. The extracted linear geological features were imported into a GIS environment and statistical analysis and representation was performed using rose diagrams. Density calculations were performed. The linear traces of faults were merged in a GIS with available geological and geophysical information (geological and geophysical maps georeferenced into ArcGIS and QGIS) such as the active faults from the Global Active Faults Database [12]. Infrastructural data were downloaded from Geofabrik [13].

Earthquakes can trigger the development of fault and fracture zones, caves, dolines and large conduits collapse, and change groundwater flows, not only because of the earthquake shock, but also because of horizontal and vertical movements. To learn about areas prone to relatively higher ground motion, earthquake data were downloaded from different sources [14], [15], [16], and the epicenters integrated into the GIS data base.

3. Geographic and Geologic Overview

As karstification processes in Central-Lebanon are strongly connected to the geologic and geographic conditions a short overview of the environmental setting is given.

3.1. Geographic Setting

The Central-Lebanon is characterized by two mountain ranges that run parallel to the coast of the Mediterranean Sea. The Mount Lebanon range borders a narrow coastal plain. The Mount Lebanon and Anti-Lebanon ranges are separated by the Bekaa valley (Figure 2a and Figure 2b). The Bekaa valley formed by a graben structure, is an elongated valley located between the Mt. Lebanon and Anti-Lebanon ranges. The NNE-SSW trending mountain ranges with their steep slopes on both sides and the Beqaa valley between the ranges, as well as the narrow costal plane are all imprints of the structural deformation during the geologic past. This complex relief results in a high spatial variability of precipitation [17] which is increasing due to climate change [18]. High intensity, but short rainfall events cause flooding, even flash floods. High precipitation is documented just to the north of Beirut with 1600 to 1700 mm of precipitation per year1 [19].
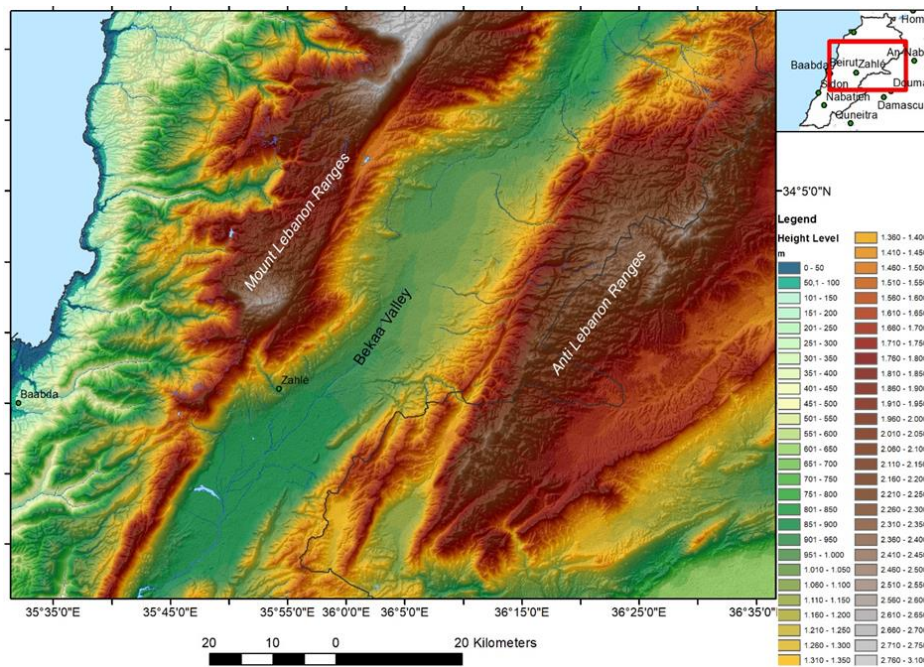
Figure 2a. Height level map based on SRTM DEM data.
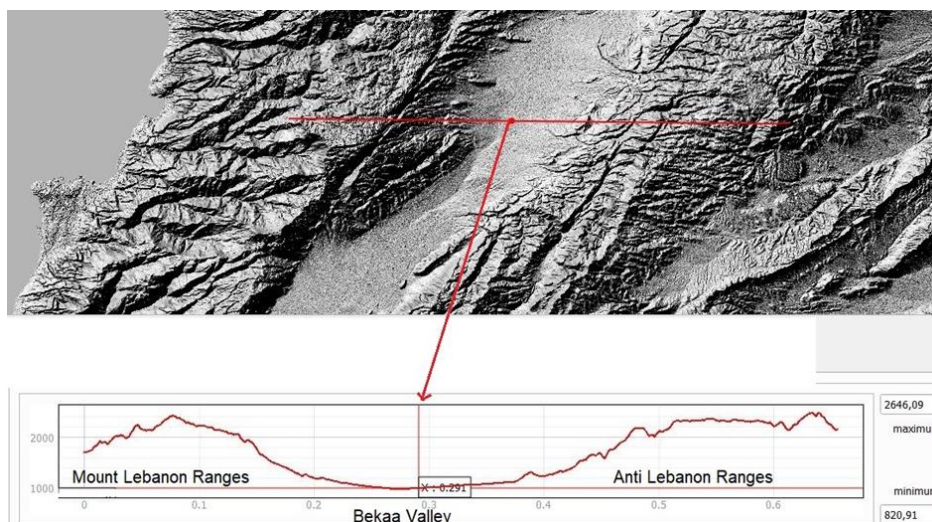
Figure 2b. Topographic cross section in W-E-direction of the Central-Lebanon.

3.2. Geologic Overview

The present structural framework of Lebanon is mainly shaped by the activity of the Dead Sea Transform fault (DSTF) that connects the ongoing opening of the Red Sea and Gulf of Aqaba to the Tauros-Zagros subduction zone. A dominant element is the Bekaa Graben with the left-lateral Yammouneh shear fault at its western boundary [2]. The Bekaa Graben is considered to be the northern extension of the Red Sea-Dead Sea-Jordan Rift Valley transform fault, the Dead Sea Transform Fault. The structural setup is mainly governed by elements resulting from the African/Arabian-European continental collision between the Upper Cretaceous and the Tertiary. Along the Yammouneh fault average late Pleistocene slip rates of 5.1 ± 1.3 mm/year were monitored based on the offset of 25-ka-old alluvial fans [20].

The geological units occurring in the study area are mainly composed of limestones /dolomites, volcanic rocks and clastic sediments. Gravity data suggest that the Beqaa valley is filled by up to 9 km of lacustrine and continental sediments with the deepest part in the central area of the valley. The timescale of the limestone formations ranges from the Lower Jurassic to Upper Cretaceous. Unroofed Jurassic units along the entire length of the Mt. Lebanon range suggests laterally constant uplift [20]. Bends and stepovers and pull-apart depressions along the strike-slip fault segments related to the Yammouneh fault trace stress heterogeneities, affecting the regional strain field. Geometrical relationships between folds and strike-slip features suggest that regional strain partitioning may accommodate a convergent component of motion between the Arabian and African plates [21].

4. Results

According to the specific properties of the remote sensing data the gained results were subdivided. Each satellite system offers different advantages (and disadvantages) regarding the evaluation results. Because of the combination of the evaluation results additional knowledge can be gained.

## 4.1. Evaluations of optical satellite data

High resolution satellite images (Bing Map, World Imagery, OrbView, Google Earth) served as base for the digitizing of surface karst features like sinkholes, enclosed depressions and poljes. Sinkholes and smaller enclosed topographic depressions are often used as detention and retention ponds. This is verified by comparative evaluations of older high resolution satellite images such as provided by Google Earth (Historical Imagery tool) showing sinkholes and closed, bowl-shaped depressions, that were later modified to detention ponds for water management. However, the mapping of sinkholes can lead to errors whenever detention basins were created without a sinkhole existence before. (A detention basin does not have a permanent pool of water. The water runs out or evaporates between rainfalls and, thus, it often remains dry).

Nevertheless, all the water-filled ponds and circular depressions visible on the satellite images were mapped as karst related depressions, assuming that the circular detention basins of the same size as sinkholes were built using the existing, natural depressions (Figure 3). In the coast-near, densely populated, sealed areas many sinkholes are not visible anymore on satellite images. Thus, errors related to the sinkhole-detection and mapping based on remote sensing data cannot be excluded.

Based on the sinkhole-shapefiles density calculation were carried out and information of the sinkhole's size derived. Most of the digitized sinkholes have small sizes between 10-60 m (Figure 4). For the better visibility buffer zones of 300 m were drawn around the sinkholes.
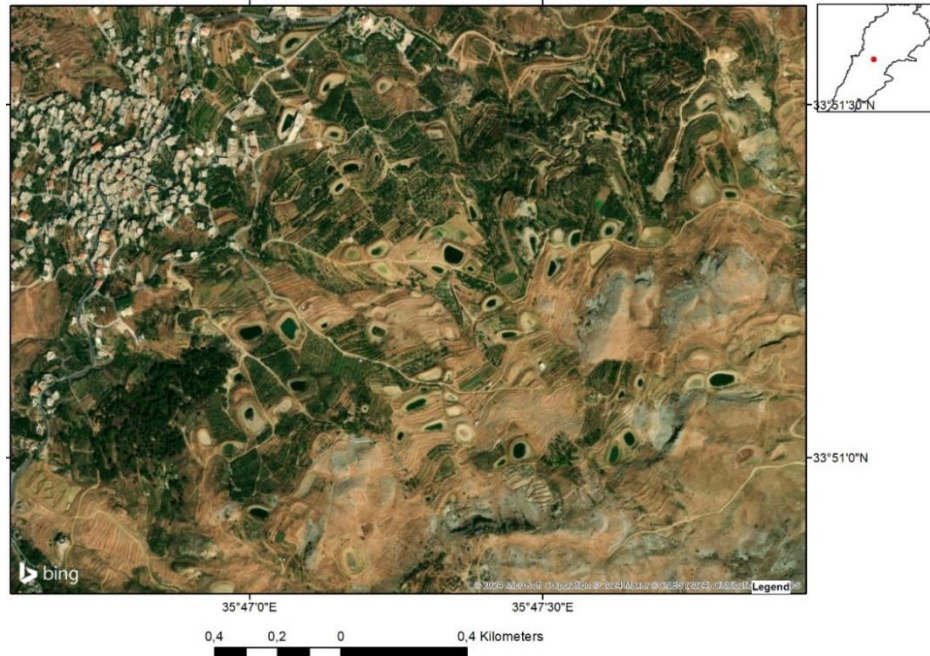
Figure 3. Sinkholes modified to detention basins to preserve water availability as visible on Bing Map images.
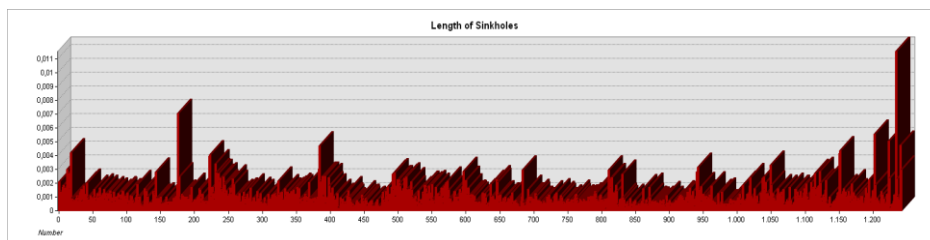
**Figure 4.** Length/diameter of sinkholes and detention basins and ponds.

When analyzing the distribution pattern of the sinkholes in Central-Lebanon, a nearly semi-circular pattern becomes visible, concentrated in a belt-like, nearly semi-circular zone, surrounding the highly fractured Cretaceous (Cenoman) limestones with brittle surfaces. This structure is bordered in the eastern part by the large Yammouneh fault zone. Most of the visible sinkholes are situated in the areas between 1500 and 2000 m height level. The areas above 2000 m height level are covered by snow for several months per year, thus, providing melt water during the warmer months. Infiltration of snow melt and surface water run-off intensifies the karstification in those areas.

Traces of major fault zones, their parallel segments, and fault related structures like pull-apart-depressions forming poljes (-flat-floored depression within karst limestones), smaller push-up ridges, and brittle surfaces are clearly visible on the different satellite images that could be verified as such by the comparison with available geologic and tectonic maps (Figure 5 and Figure 6) [22], [23], [2], [3], [24]. Understanding the impact of deformation patterns on the hydraulic properties of the rock is essential for a better knowledge of karst processes. Uplifting

movements, intrusions of volcanic rocks, earthquake shock, and high tectonic stress have contributed to the development of the brittle surfaces supporting dissolution processes and collapses in the lime- and dolostones.

Brittle surfaces are characterized by the rough surfaces including small, parallel valleys and ridges, shallow, bowl-shaped depressions and sinkholes, often in a linear arrangement (uvalas). Karstification processes contribute to the sculpturing and modelling of the brittle surfaces by creating the small enclosed depressions, poljes, sinkholes and karren surfaces.

The brittle surfaces are concentrated along the SSW-NNE striking fault zones. The brittle surfaces can be observed along the SSW-NNE oriented major fault zones, the Yammouneh strike-slip fault, of the Bekaa valley and their intersections with SW-NE striking faults (Figure 6). An overview of the digitized fault zones, brittle surfaces and karst features is shown in Figure 5 and Figure 6. Various types of deformation due to geodynamic activity could be observed (Figure 7).
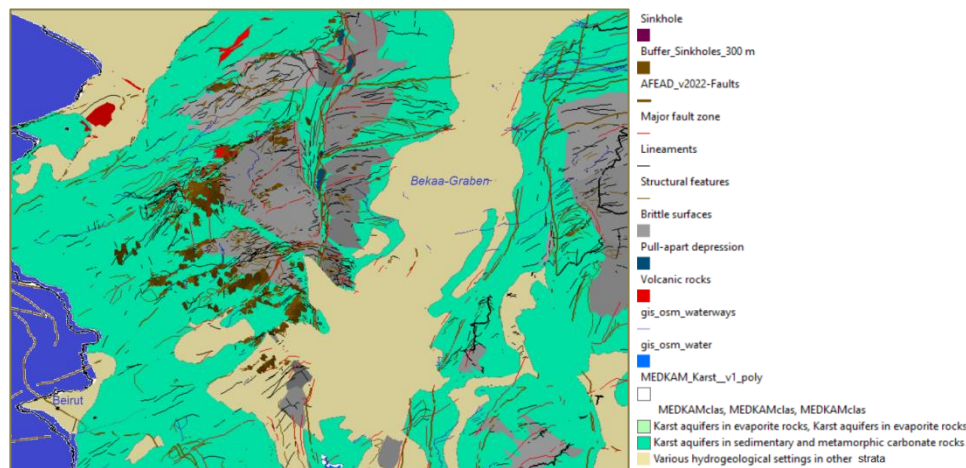
Figure 5. 3D perspective view of the structural pattern of Central-Lebanon looking towards north.

The information of the volcanic rocks war derived from the geologic map [22]. Known faults (brown lines) were included from [12] and [25].

As there exist outcrops of volcanic intrusions in this area (Figure 5), it has still to be further investigated to which extent the uprise of magmatic bodies underneath and intrusion into the limestones and dolomites has caused thermal altering, metamorphism and fracturing. Magmatic intrusions (here mainly basalts) can form a hindrance and natural barriers for the groundwater flow in the affected areas, especially when occurring as dykes.

The degree of brittleness in the limestones is mainly controlled by their mineralogic composition. It increases with higher quartz and dolomite content, whereas an increase in the clay content represents an increase in ductility [26]. The brittle-ductile transition depends on grain size and porosity. Porous carbonate rocks are often mechanically weak, heterogeneous at multiple scales, sensitive to effective stress changes, and to the chemistry of the fluid saturating the pore space. (-Brittle deformation happens when rocks fail as rigid solids. The rocks will break, rather than bend, under these conditions to produce fractures. Brittle deformation occurs along discrete planes in the rock instead of involving the rock body as a whole. Later, fractures can be places where material is removed as a result of rock dissolution, or minerals can grow in the open fracture spaces.) [27]. The several months long duration of

snow cover and, thus, later the melting water contributes to dissolution processes and to the modeling the brittle surfaces. Due to the dense drainage pattern, surface water is "trapped" in the small, narrow valleys. They function obviously to funnel rainfall and downwards runoff and, thus creating rillen-karren. The dissolution conditions in the limestones within the small channels support the development of closed, bowl-shaped depressions, often arranged as uvalas, and of elongated poljes.
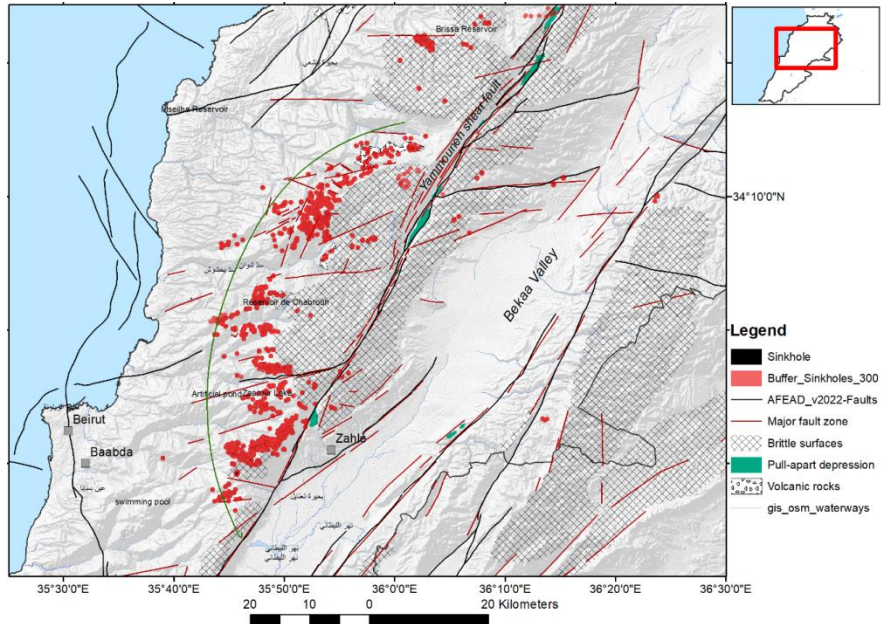
Figure 6. Structural evaluation of satellite data and overview of brittle surfaces in Central-Lebanon. The green line indicates the nearly semi-circular outline of the distribution of sinkholes. Faults from the Global Active Faults Database [12] were included.
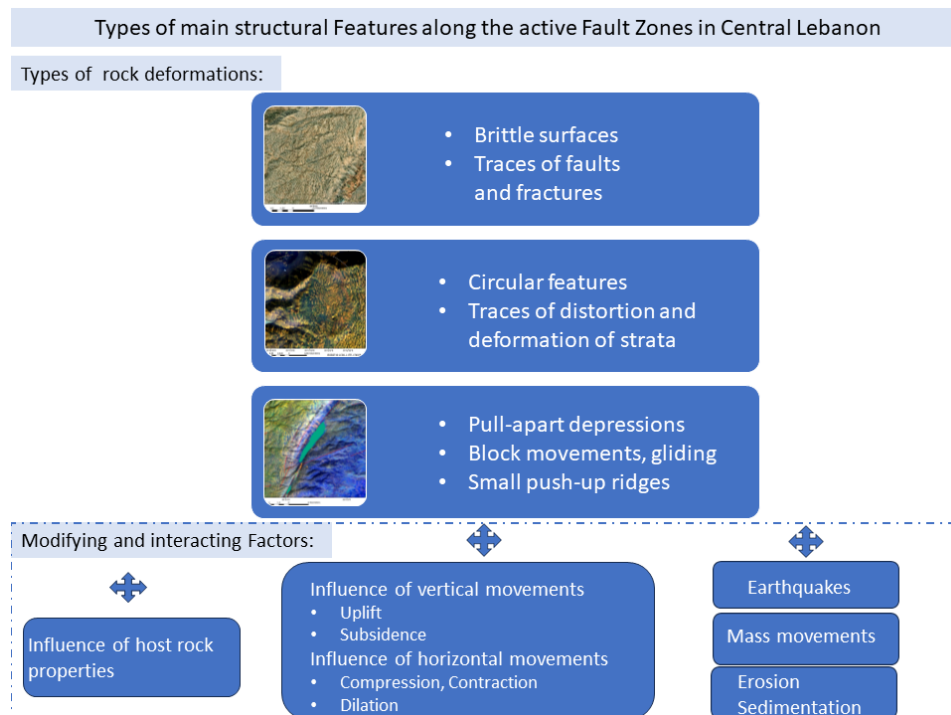
Figure 7. Types of deformation monitored by the evaluation of different satellite data.

The brittle surfaces vary in their brittle density as shown in Figure 8 (areas 1-3). The drainage pattern allows the detection of the structural setting. The orientation of the surface fault and fracture pattern is tracing the stress situation changes.

The small, narrow valleys and ridges are clearly visible on the Modified Normalized Difference Water Index (MNDWI) image result created with the SNAP software (Figure 9a). The MNDWI image reveals information related to soil moisture, in this case of snow cover. The small valleys and depressions, still covered by snow, appear in blue colors. The red lines represent the Yammouneh shear fault segments.
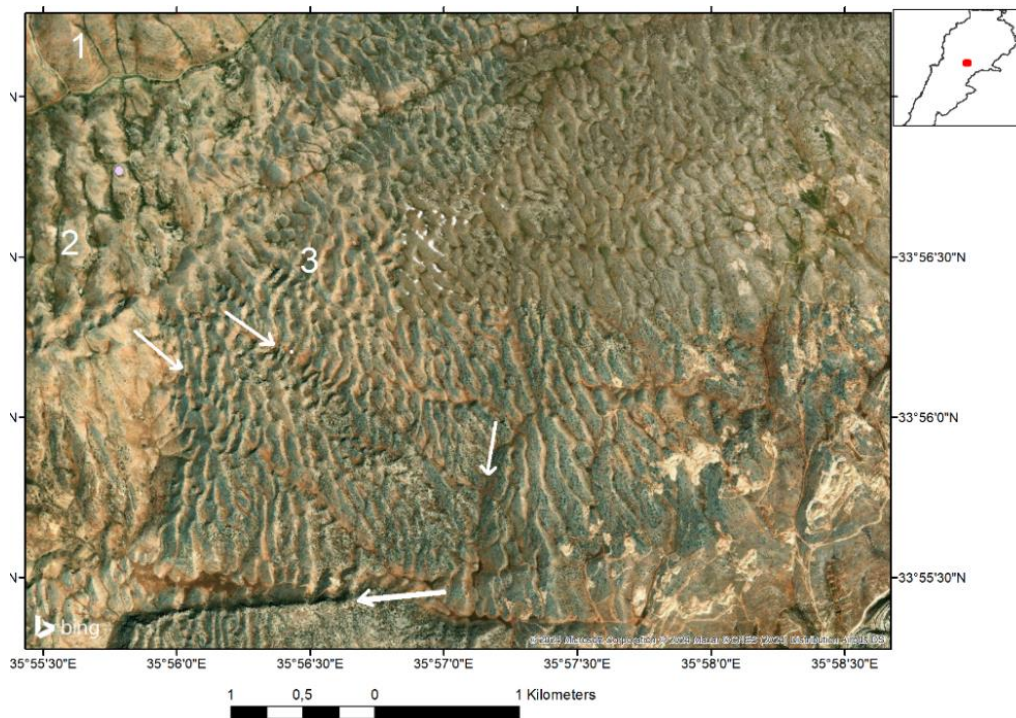
Figure 8. Brittle surfaces of outcropping limestones with different brittle intensity patterns 1- lower density, 2 and 3 – higher density) intersected by faults (arrow).

The drainage pattern and orientation reflect the stress situation clearly [28]. The majority of the small segments are oriented parallel to the SSW-NNE striking Yammouneh shear fault. The rose diagram of Figure 9c, derived from the drainage orientation analysis based on ALOS PALSAR DEM data (calculated in QGIS), shows the main directions of the drainage segment orientations.

The dense fracture pattern facilitates the infiltration of surface water and, thus, karstification processes such as towards karren karst forms (rill-like erosional form of limestone solution). Sinkholes and springs appear to be concentrated at the western border of the nearly semi-circled outline of the limestones with brittle surfaces in the north of the city of Zahle (Figure 10). The information of the springs was provided by [3] and [25]. Their distribution is influenced by SW-NE and SSW-NNE striking fault zones. The distribution pattern of sinkholes is also an important factor for the water recharge, especially for those sinkholes forming uvalas along predominant alignments. These alignments are usually tracing faults that create high permeability and porosity zones in the affected areas [1].
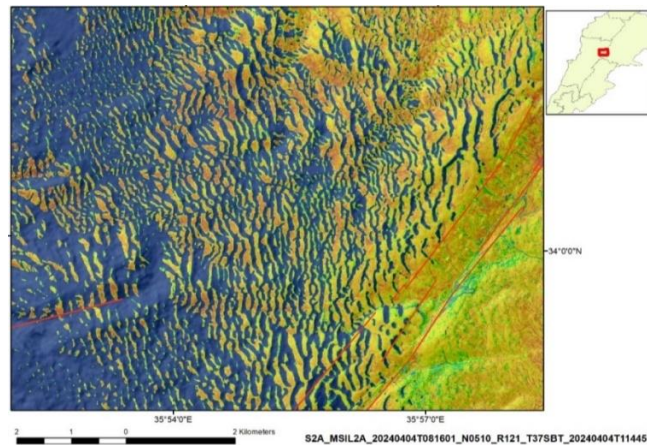
Figure 9a. Brittle surfaces visible on a Modified Normalized Difference Water Index (MNDWI).
MNDWI= (Green - SWIR)/(Green + SWIR) image, color-coded, derived from the
Sentinel 2 satellite data acquired on 24.04.2024.

b)   c)
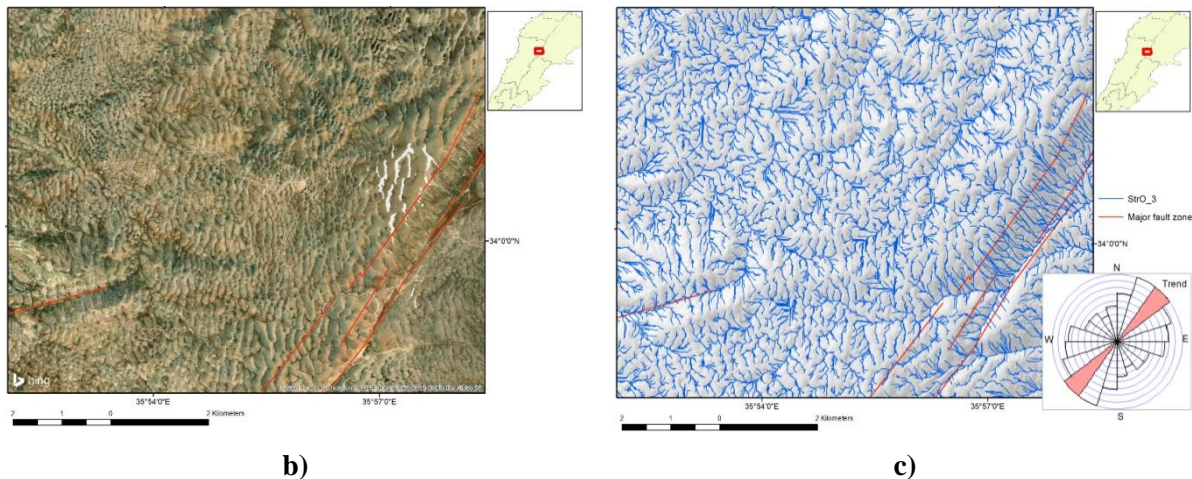
Figure 9. b) Bing Map scene of a brittle surface and **c)** drainage pattern tracing the structural pattern
and karren landforms and the derived drainage segment orientation (trend shown in red colors)
in the west of the Yammouneh fault zone (red lines).
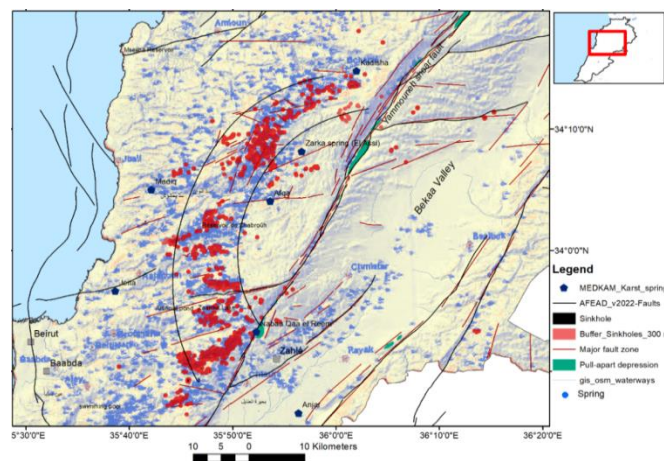
Figure 10. Distribution of springs according to [3] and [25].
Sinkholes occur concentrated within a nearly semi-circular belt-zone.

Earthquake epicenters were included into the investigation [14,15,16] and their density calculated (Figure 11 a and b). When analyzing the earthquake pattern during the two last decades it becomes obvious that stronger ground motions after earthquakes must have contributed to the intense geomechanically stress within the limestones resulting in a dense fracture and deformation pattern and, obviously, as well as to long term horizontal and vertical movements. Most of the earthquakes happen in depths below 10 km.
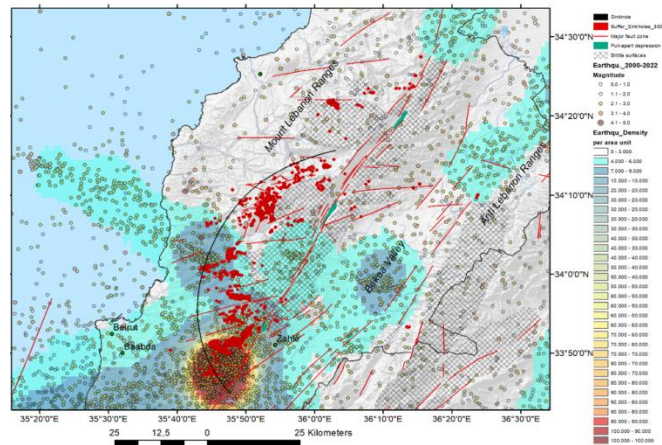
Figure 11a. Distribution of sinkholes, brittle surfaces and earthquake density.
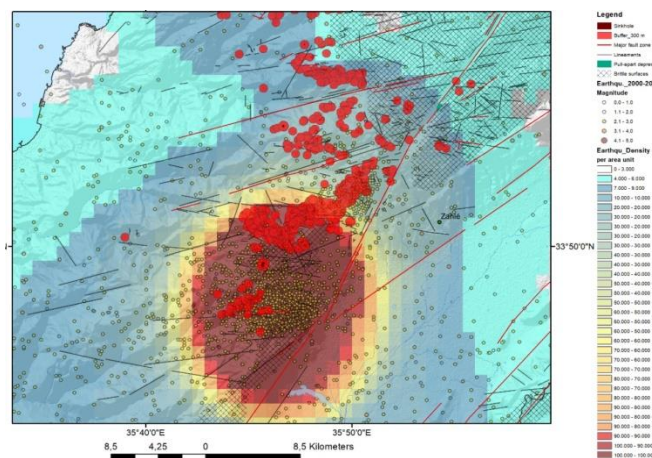
b) Amplification of the southern part of (a)

Figure 11b. Earthquake density calculation. **(a)** Distribution of sinkholes, brittle surfaces and earthquakes.

(b) Amplification of (a). Sinkholes (red) occur concentrated along the intersection of

SW-NE and SSW-NNE striking fault zones with a higher earthquake density.

The thermal bands of Landsat satellites support the detection of circular features (Figure 12). Their origin might be related to larger sinkholes or to local uprise of magmatic bodies up-doming the strata above. Outcrops of Cretaceous and Tertiary volcanic rocks (mainly basalts, often as dyke intrusion) are documented on the geologic maps of this region, occurring in the "belt zone" of sinkhole concentration. In case of volcanic influence, rising pressure and temperature due to limestone–magma interaction might be the reason for the denser brittleness. Hydrothermal activity related to volcanism with increased dissolution obviously led to the concentration of karst features near volcanic intrusions. Traces of ring structures as visible on the Landsat scene (Figure 13, including in

the RGB image the thermal bands 7 and 10) might be explained by circular and ellipsoidal zones around collapse structures after dissolution processes in limestones as well. The corresponding Google Earth scene of the circular structure is presented in Figure 14. Water-filled, small circular depressions are visible as dark spots. Enclosed, bowl-shaped depressions show partly a linear arrangement. Not all of them seem to be sinkholes. To clarify their properties field investigations are necessary.
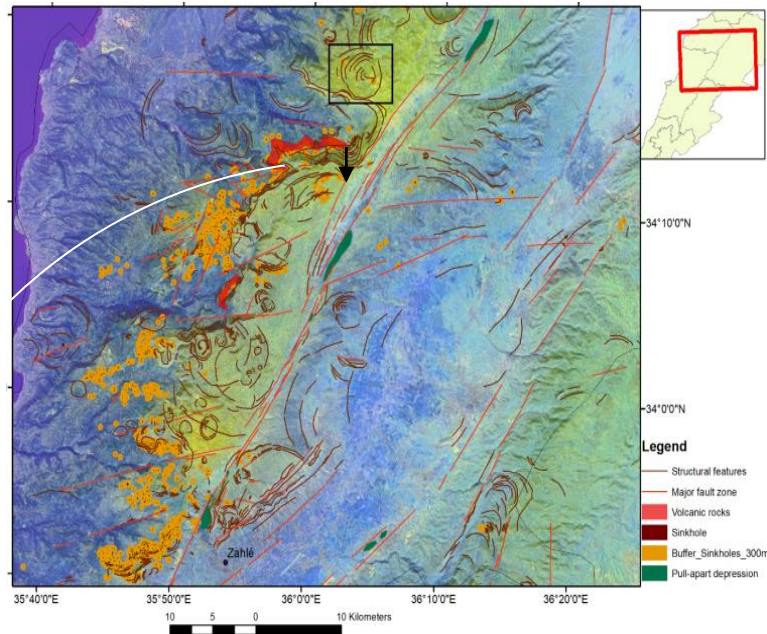
Figure 12. Structural features and sinkhole distribution concentrated in a nearly semi-circlar pattern visible on a Landsat 8 scene of the central Bekaa valley. The position of the circular structure shown in Figure13 and Figure 14 is indicated by the black rectangle.
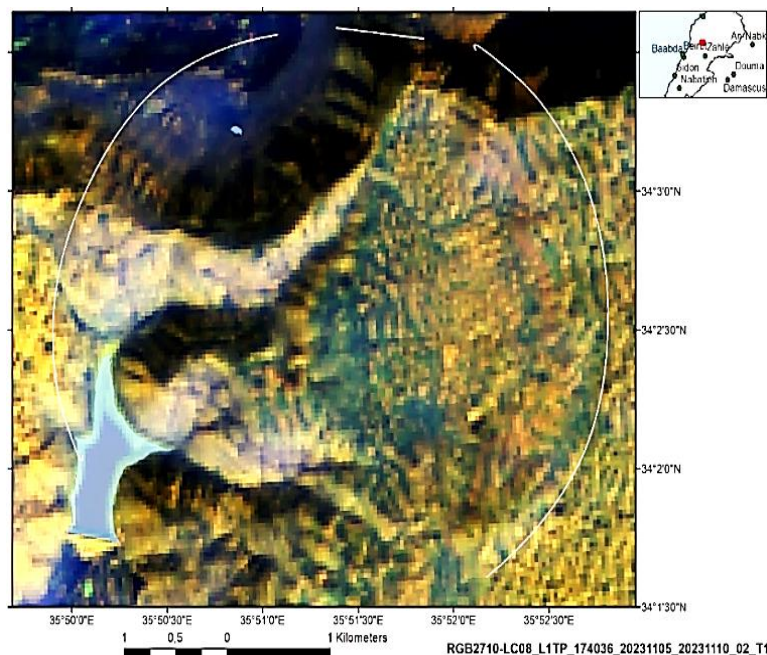
Figure 13. Circular structure visible on a Landsat 8-scene (30 m spatial resolution) situated within limestones with brittle surfaces.

Figure 14. 3D perspective Google Earth view (position: 34°02'22.97" N 35°52'10.15" E) of the central part of the circular structure, partly covered by snow.

4.2. Evaluations of Radar Data

Although radar shadow, foreshortening and lay-over effects on the radar images have to be taken into account because of the high mountain terrain conditions, some additional information can be derived as demonstrated in Figure 15 and Figure 16. Closed circular depressions can be detected on the L-Band images of the ALOS PALSAR satellite that do not appear on optical satellite images (Figure 16, white arrows).
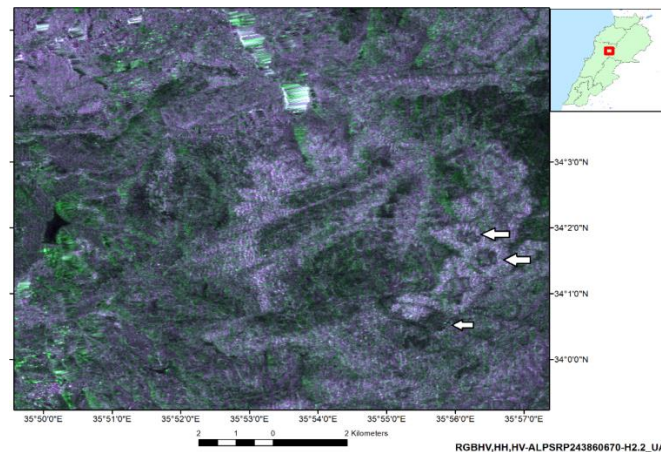
Figure 15. ALOS PALSAR radar scene tracing circular features.
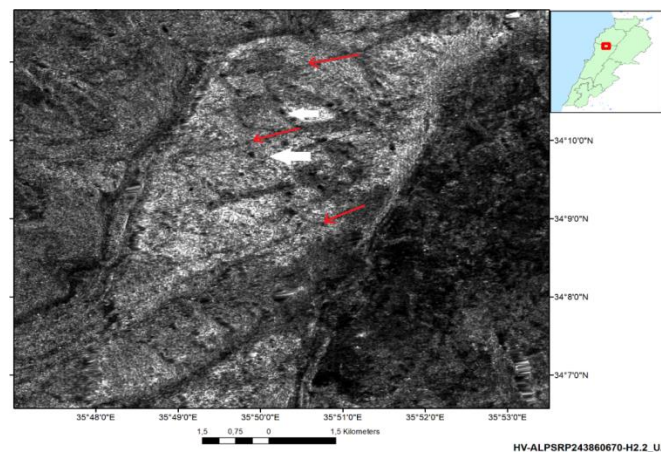
Figure 16. Radar scene (ALOS PALSAR) revealing smaller sinkholes (black spots indicated by white arrows) and fracture zones (dark lines, indicated by red arrows).

4.3. Evaluations of DEM Data

SRTM, ASTER (both about 30 m spatial resolution) and ALOS PALSAR (about 12.5 m resolution) DEM Data were processed in ArcGIS using the Spatial Analyst tools to derive different morphometric maps, among them the delineation of drainage basins and morphologic watersheds (Figure 17). However, as karst catchment areas comprise a complex water transport system characterized by the heterogeneity of surface and underground karst forms, this drainage basin map is covering only the information of surface water-runoff.

The drainage pattern (stream order according to Strahler) was derived as well from the DEM data (Figure 18). To get an idea where the highest surface water input can be expected, the drainage density was calculated based on the drainage shapefiles derived from ALOS PALSAR DEM data (Figure 18). (- The analysis of drainage network density represents the sum of fluvial segment length inside a grid cell). Higher drainage densities can be observed along the larger fault zones, especially along the Yammouneh shear fault, and along a nearly semi-circular zone with a width of about 5 – 10 km in the west of the Bekaa valley, as indicated in Figure 18b. The visible sinkholes occur concentrated within the same zone. The highest concentrations of the drainage segments are visible on Figures 18 a and b in the northeast of the city of Zahle. The higher the meteorological surface water input, the more intense get the karstification processes and the higher is the groundwater recharge potential.
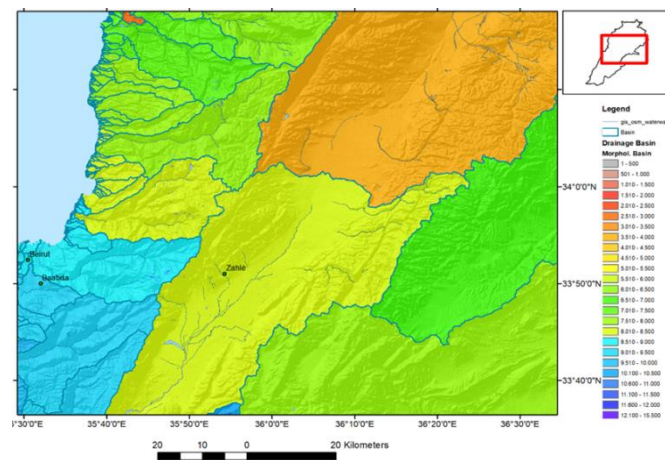
Figure 17. Drainage basins indicating morphologic watersheds.
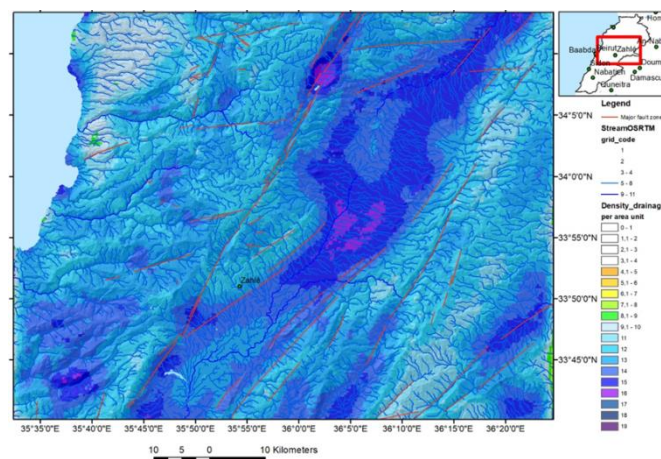

Figure 18a. Drainage density calculation derived from ALOS PALSAR DEM data.
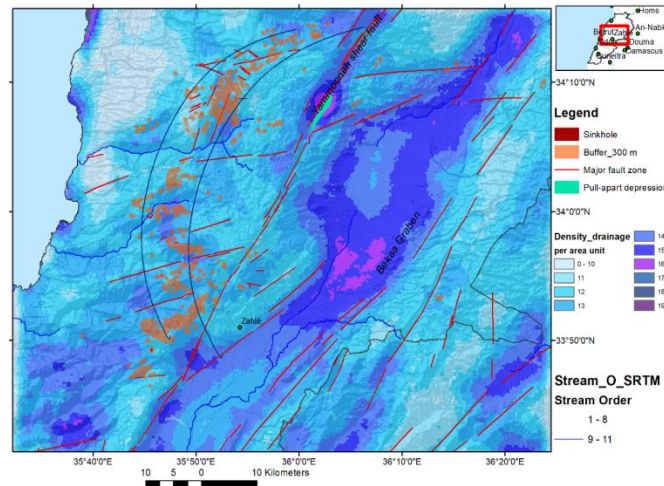
Figure 18b. Drainage density calculation merged with the occurrence of visible sinkholes.

Some morphometric factors influence the disposition to be prone to relatively more intense karstification such as height levels, slope orientations, slope degree, and curvature of the terrain, etc. A weighted overlay procedure can be carried out for the detection of areas with higher susceptibility to flash floods and to higher surface water input and infiltration by extracting first causal/preparatory factors and, then, by aggregating these morphometric factors (lowest local height level, slope degrees $< 5°$, curvature $= 0$, aspect $= (-1)$ flat) in the weighted overlay-tool of ArcGIS (Figure 19). The result of the aggregation of these morphometric factors shows areas susceptible to higher surface water input after precipitations and even susceptible to flash floods due to their morphologic disposition. This approach is useful as well to detect pull-apart depressions, poljes and the morphometric properties of the larger valleys.
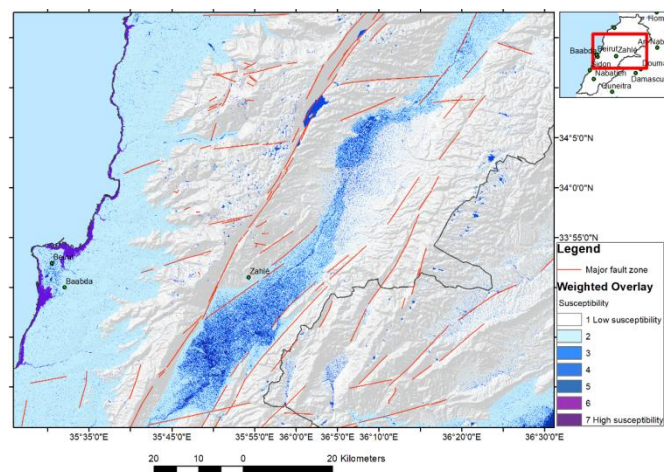

Figure 19. Weighted overlay approach in ArcGIS - Susceptibility to higher surface water input and infiltration (4 -7) due to the local morphometric disposition.

The exposition of the slopes plays an important role when considering the main rain bearing air masses, clouds and wind directions, here coming from SW and W. West winds arriving from the Mediterranean Sea are often changed in their directions towards north or south due to the hindrance of the high mountain ranges, the Mount Lebanon ranges and Anti Lebanon ranges, forming a wind barrier (Figure 20). Because of the orographic situation and

effects the slopes oriented towards SW get more rain (Figure 21) as air masses are forced to flow over the high topography. Whenever air rises over the Mount Lebanon ranges, it cools, and water vapor condenses. As a result, the rain occurs concentrated on the windward side of the mountain range. Rainfall increases with elevation in the direction of wind directions and cloud tracks. Sinkholes in the limestones occur exactly where the highest precipitations were measured (Figure 22).

The majority of the sinkholes are situated luv-wards in the west of the highest areas of the Mount Lebanon range. Most of the visible sinkholes are situated along slopes oriented towards SW to W what can be verified by aspect maps. By calculating aspect maps from DEM data, the slopes oriented toward W and SW can be derived. Thus, the relationship between the exposition of slopes to rain-bearing clouds and relatively higher surface water input (leading to more intense karstification) and the occurrence of sinkholes can be visualized.
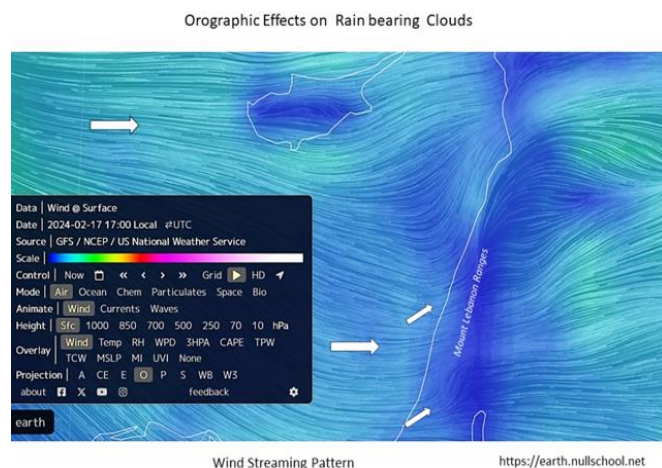

Figure 20. Wind pattern (19.03.2024) indicating the orographic effects of the Lebanon mountains by directing the western winds towards north. Wind data were downloaded from [29].
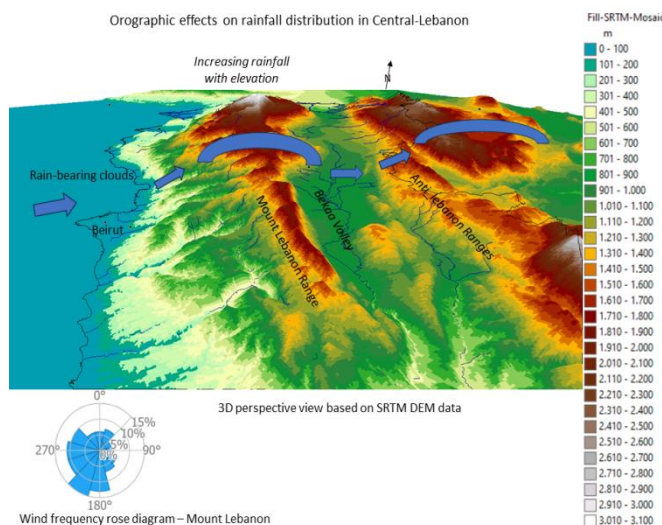

Figure 21. Orographic effects on the precipitation amount (schematically represented by blue arrows) considering the main wind directions.

Rose diagram: https://globalwindatlas.info/en/area/Lebanon/Mount%20Lebanon
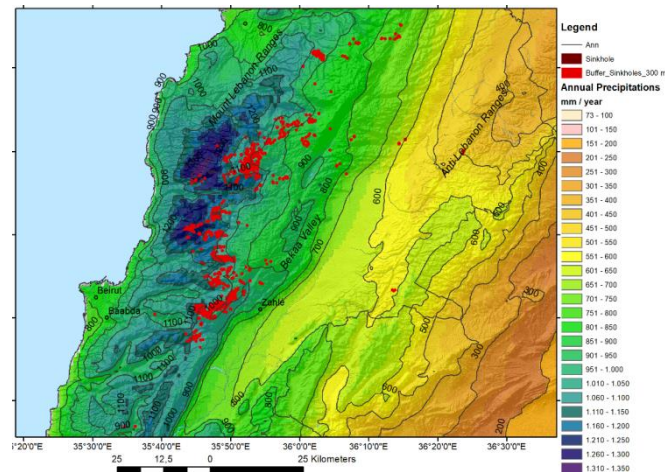
Figure 22. Annual precipitations according to WorldClim version 2.1 climate data for 1970-2000 released in 2020 [19] with 30 seconds (~1 km2) spatial resolution.

The orientation of slopes derived from DEM data by calculating aspect maps is shown in Figure 23.
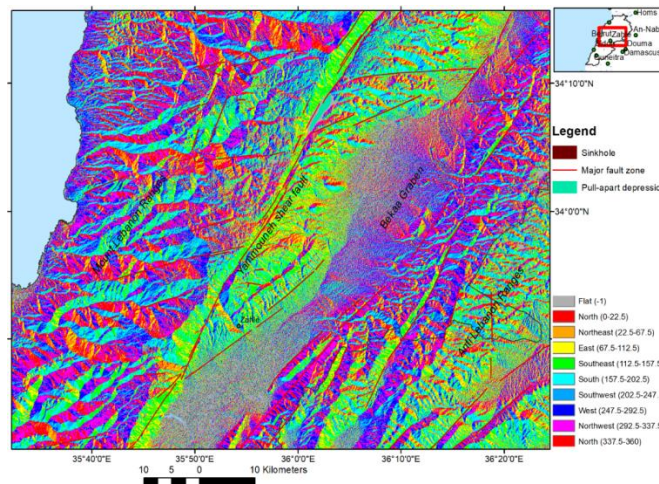

**Figure 23a.** Aspect map of Central-Lebanon based on SRTM DEM data.
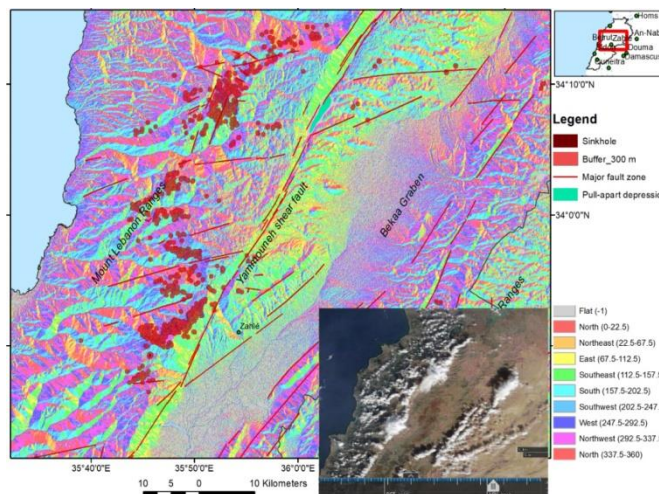
Figure 23b. Aspect-map combined with the mapped sinkholes and a typical cloud situation image (acquired: 22.11.2022) [30].

Pull-apart depressions and basins become visible when subtracting the original DEM data from the Fill-DEM data created in ArcGIS using the tools in the Spatial Analyst extension. The first step used the "Fillsink" algorithm from the ArcMap software (identifying the point or set of adjacent points surrounded by neighbors with higher elevation and rises to the lowest value on the depressions boundary). This procedure then fills all depressions in the DEM, including both those generated from data errors (spurious artifacts) and those that record real topographic features, such as karst depressions (dolines). The second step was to extract the sink depths in these areas by differencing the maps between the sink-filled ("depressionless" DEM) and original DEM. The difference image can highlight the different depressions, including the karst enclosed depressions. Figure 24 shows the result of such a subtraction of SRTM-DEM from Fill-SRTM DEM data. The elongated pull-apart-depressions along the left-lateral shear zone appear very precisely. This method can be applied to detect larger sinkholes and poljes as well whenever the sizes depths of the bowl-shaped and elongated depressions are distinct enough to be visible (Figure 25). However, the DEM spatial resolution (SRTM and ASTER DEM - 30 m, ALOS PALSAR DEM - 12.5 m) is not sufficient enough to detect the smaller sinkholes and enclosed depressions. Smaller depression cannot be detected as demonstrated by the Google Earth scene with depressions that are not visible on the calculated difference map (Figure 25).
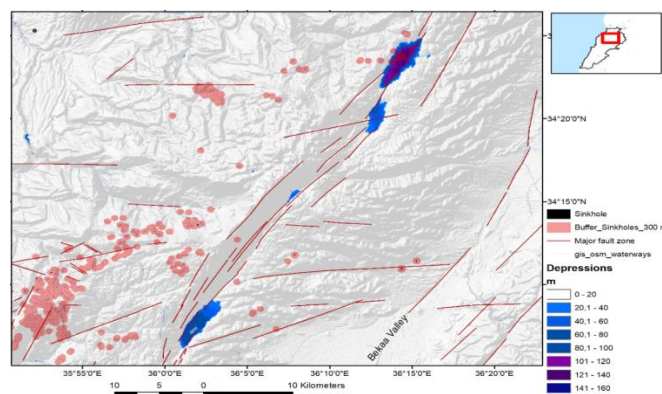
Figure 24. Detection of pull-apart depressions (blue) based on ALOS PALSAR DEM data using the difference between (Fill-DEM – DEM).
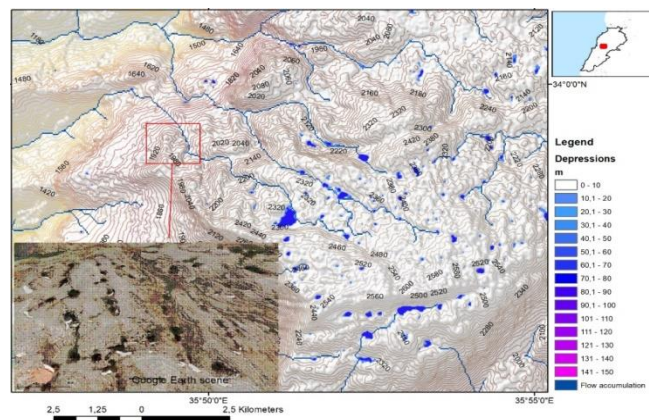

Figure 25. Detection of larger depressions (blue) by calculating (ALOS PALSAR_Fill DEM – DEM). Smaller depressions along the narrow valleys and ridges are not visible due to the limited spatial resolution of the DEM data.

5. Conclusion

The multisource approach presented in this article contributes to a further knowledge of the development of karst in this region. The different satellite and geodata support the better understanding of the occurrence and distribution pattern of surface karst features in Central-Lebanon as far as they are visible on the satellite images. The use of morphometric factors, especially the spatial distribution of the drainage network, drainage density calculations, orientation analysis, combined with tectonic lineaments data and lithologic layers provide additional knowledge related to the hydrogeological characterization of the region. The evaluations of the different satellite data reveal the existence of structural features such as ring structures, that, sometimes, become only visible on the thermal bands of the Landsat images or on radar images.

Several factors seem to have an influence on the spatial distribution and concentration of karst features as summarized in Figure 26: Occurrence of limestones, heights > 1500 m, slopes oriented towards W, SW, NW, slopes with slope degrees between 40-70°, annual precipitations above 1000 mm/year, larger fault and fracture zones (especially when intersecting each other) and a higher earthquake density. The secondary effects of earthquakes in this area and their characteristics have to be considered, depending on their magnitudes, depths and spatial concentrations. The predominantly shallow earthquakes below 10 km depth with higher magnitudes have an impact on the rock properties, especially on the development of fractures and faults. Thus, in areas with a higher earthquake density more surface karst features can be observed. Larger fault and fracture zones influence the hydrogeologic conditions due to the higher water permeability in the affected areas. The analyses of the different satellite images and of DEM data contribute to the detection of areas with higher surface water input which is important for the groundwater recharge.
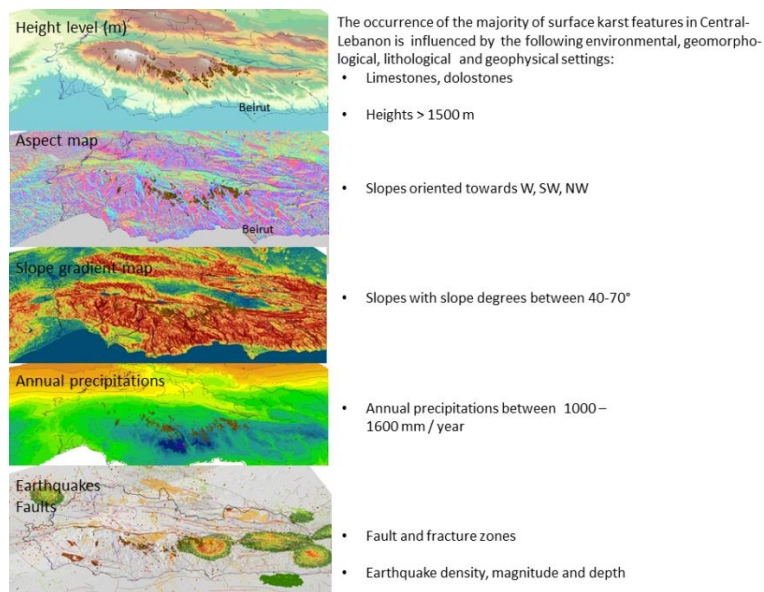
Figure 26. Main factors influencing the occurrence of sinkholes (brown spots) and other surface karst features in Central-Lebanon.

As karst water resources are important for the water supply and economic development in Lebanon, more detailed research of the specific local situation in the karst areas is carried on. The structural evaluations of remote sensing

data can support the detection of fault and fracture zones in karst areas with influence on groundwater permeability. However, high resolution image and DEM data are required for a more detailed analysis such as gained by drones or by the LIDAR techniques. They are necessary as well for the detection of sinkholes. Future research should include the investigation of the impact of magmatic intrusions into the limestones in Central Lebanon and, as consequence, on aquifers. Long term horizontal and vertical movements play an important role, too, affecting the development of fracture zones. More geodetic data have to be considered. Further on, the effects of climate changes with a relatively higher frequency of extreme weather events have to be monitored in the karst areas such as extreme draughts or flash floods and their impact on the karst aquifers.

References

[1] Shaban, A., & Darwich, T. (2011). The Role of Sinkholes in Groundwater Recharge in the High Mountains of Lebanon. Journal of Environmental Hydrology, 19.

[2] Rizk, J.A., & Margane, A. (2011). Mapping of Surface Karst Features in the Jeita Spring Catchment. Special Report No.7, Mapping of Surface Karst, Technical Cooperation, Project No. 2008.2162.9, Republic of Lebanon, Council for Development and Reconstruction, CDR, Beirut and Federal Republic of Germany, Federal Institute for Geosciences and Natural Resources (BGR), Hannover, Pages 59.

[3] Ministry of Energy and Water of the United Nations Development Programme (MoEW and UNDP) (2014). Assessment of Groundwater Resources of Lebanon. Report. https://www.undp.org/lebanon/publications/assessment-groundwater-resources-lebanon.

[4] US Geological Survey, Earth Explorer. Available online: https://earthexplorer.usgs.gov/ (Accessed: December 2023–April 2024).

[5] European Space Agency (ESA), Copernicus Browser. Available online: https://dataspace.copernicus.eu/.

[6] National Aeronautics and Space Administration (NASA), Earth Data, Earth Science Data Systems (ESDS) Program. Available online: https://search.earthdata.nasa.gov/search.

[7] Japan Aerospace Exploration Agency (JAXA), PALSAR-2 Global Forest/Non-forest Map "2022". Available online: https://www.eorc.jaxa.jp/ALOS/en/palsar_fnf/data/2022/map.htm.

[8] Fletcher, K. (ed.) (2005). Spaceborne Radar applications in Geology – An introduction to imaging radar, and application examples of ERS SAR in Geology and Geomorphology. European Space Agency, ESA TM-17, 234 Pages.

[9] Booysen, R., Gloaguen, R., Lorenz, S., Zimmermann, R., & Nex, P.A.M. (2021). Geological Remote Sensing. Encyclopedia of Geology (Second Ed.), Pages 301–314. https://doi.org/10.1016/B978-0-12-409548-9.12127-X.

[10] NASA Earth Data, Alaska Satellite Facility (ASF), Data Search Vertex. Available online: https://search.asf.alaska.edu/#/.

[11] JAXA, Earth Observation Research Center, Global PALSAR-2/PALSAR/JERS-1 Mosaics and Forest/Non-Forest Maps. Available online: https://www.eorc.jaxa.jp/ALOS/en/dataset/fnf_e.htm.

[12] Global Active Faults Database (GEM GAF-DB). Available online: https://blogs.openquake.org/hazard/global-active-fault-viewer/.

[13] Geofabrik's free download server, Download OpenStreetMap data for this region: Lebanon. Available online: http://download.geofabrik.de/asia/lebanon.html.

[14] International Seismological Centre (ISC) Bulletin: interactive event catalogue search. https://doi.org/10.31905/D808B830. Available online: http://www.isc.ac.uk/iscbulletin/search/catalogue/interactive/.

[15] USGS, Search Earthquake Catalog. Available online: https://earthquake.usgs.gov/earthquakes/search/ (Accessed: March 2024).

[16] Euro-Mediterranean Seismological Centre (EMSC), Earthquake data. Available online: http://www.emsc-csem.org/ (Accessed: February 2024).

[17] Mohammad, M. (2015). Hydrology of Lebanese catchments in the Mediterranean context. Environmental Sciences. AgroParisTech, HAL Id: tel-01262314. https://theses.hal.science/tel-01262314v2.

[18] Lemenkova, P. (2022). Geomorphology of the Beqaa Valley, Lebanon and Anti-Lebanon Mountains. Acta Scientifica Naturalis (ASN), 9(1): 1–22. doi: 10.2478/asn-2022-0002.

[19] Global climate and weather data – WorldClim, version 2.1 climate data for 1970-2000 released in 2020. Available online: https://www.worldclim.org/data/worldclim21.html.

[20] Fedorik, J., Maesano, F.E., & Afifi, A.M. (2022). A validated geomechanical model for the strike-slip restraining bend in Lebanon. Scientific Reports, 12: 20071. https://doi.org/10.1038/s41598-022-24718-0.

[21] Gomez, F., Khawlie, M., Tabet, C., Darkal, A.N., Khair, K., & Barazangi, M. (2006). Late Cenozoic uplift along the northern Dead Sea transform in Lebanon and Syria. Earth and Planetary Science Letters, 241(3–4): 913–931. https://doi.org/10.1016/j.epsl.2005.10.029.

[22] Dubertret, L. (1955). Geological map of Lebanon at 1.50.000. Republic of Lebanon, Minister of public affairs, Beirut, Lebanon.

[23] Nemer, T., Gomez, F., Al Haddad, S., & Tabet, C. (2008). Coseismic growth of sedimentary basins along the Yammouneh strike-slip fault (Lebanon). Geophys. J. Int., 175: 1023–1039. https://doi.org/10.1111/j.1365-246X.2008.03889.x.

[24] Lateef, A.S.A. (2007). Geological History of the Bekaa Valley. Second International Conference on the Geology of the Tethys, Cairo University, Pages 391–402.

[25] Xanke, J., Goldscheider, N., Bakalowicz, M., Barberá, J.A., Broda, S., Chen, Z., Ghanmi, M., Günther, A., Hartmann, A., Jourde, H., Liesch, T., Mudarra, M., Petitta, M., Ravbar, N., & Stevanovic, Z. (2022). Mediterranean Karst Aquifer Map (MEDKAM), 1: 5,000,000. https://doi.org/10.25928/MEDKAM.

[26] Yu, S., Deng, J., Deng, H., Gao, F., & Li, J. (2020). Brittle Characteristic and Microstructure of Sandstone under Freezing-Thawing Weathering. Advances in Civil Engineering, 12 Pages. https://doi.org/10.1155/2020/889327.

[27] Sari, M., Sarout, J., Poulet, T., Dautriat, J., & Veveakis, M. (2022). The Brittle–Ductile Transition and the Formation of Compaction Bands in the Savonnières Limestone: Impact of the Stress and Pore Fluid. Rock Mechanics and Rock Engineering, 5: 6541–6553. https://doi.org/10.1007/s00603-022-02963.

[28] Doumit, J.A. (2017). Discovery of Crustal Movements areas in Lebanon: A study of Geographical information systems. Bull. Env. Pharmacol. Life Sci., 6(5): 48–52. https://bepls.com/april_2017.html.

[29] Earth.nullschool.net, GEOS-5 data provided by the Global Modeling and Assimilation Office (GMAO) at NASA Goddard Space Flight Center through the online data portal in the NASA Center for Climate Simulation. Available online: https://earth.nullschool.net/?fbclid=IwAR0nOVzGkeE73z7qvSy21_Ve2eK7AMiNKK1UTpTPG5JCa2l6gXXOMnvmDFs.

[30] NASA Worldview. Available online: https://worldview.earthdata.nasa.gov/?v=34.55071109076683,33.50142870892774,36.99411267310432,34.77135453132683&t=2022-11-02-T20%3A37%3A11Z).